7-19-2010

Detailed Microscopic Analysis of Self-interstitial Aggregation in Silicon. II. Thermodynamic Analysis of Single Clusters

Sumeet Kapur
University of Pennsylvania, kapurs@seas.upenn.edu

Alex M. Nieves
University of Pennsylvania, nievesam@seas.upenn.edu

Talid Sinno
University of Pennsylvania, talid@seas.upenn.edu

Detailed Microscopic Analysis of Self-interstitial Aggregation in Silicon. II. Thermodynamic Analysis of Single Clusters

Abstract

We analyze results generated by large-scale molecular-dynamics simulations of self-interstitial clusters in crystalline silicon using a recently developed computational method for probing the thermodynamics of defects in solids. In this approach, the potential-energy landscape is sampled with lengthy molecular-dynamics simulations and repeated energy minimizations in order to build distribution functions that quantitatively describe the formation thermodynamics of a particular defect cluster. Using this method, a comprehensive picture for interstitial aggregation is proposed. In particular, we find that both vibrational and configuration entropic factors play important roles in determining self-interstitial cluster morphology. In addition to the expected role of temperature, we also find that applied (hydrostatic) pressure and the commensurate lattice strain greatly influence the resulting aggregation pathways. Interestingly, the effect of pressure appears to manifest not by altering the thermodynamics of individual defect configurations but rather by changing the overall energy landscape associated with the defect. These effects appear to be general and are predicted using multiple, well-tested, empirical interatomic potentials for silicon. Our results suggest that internal stress environments within a silicon wafer (e.g., created by ion implantation) could have profound effects on the observed selfinterstitial cluster morphology.

Disciplines

Biochemical and Biomolecular Engineering | Chemical Engineering | Engineering

Comments

Suggested Citation:
Kapur, S., A.M. Nieves and T. Sinno. "Detailed Microscopic Analysis of Self-interstitial Aggregation in Silicon. II. Thermodynamic Analysis of Single Clusters." *Physical Review B*. 82, 045206.

Detailed microscopic analysis of self-interstitial aggregation in silicon. II. Thermodynamic analysis of single clusters

Sumeet S. Kapur, Alex M. Nieves, and Talid Sinno*
Department of Chemical and Biomolecular Engineering, University of Pennsylvania, Philadelphia, Pennsylvania 19104, USA
(Received 18 April 2010; published 19 July 2010)

We analyze results generated by large-scale molecular-dynamics simulations of self-interstitial clusters in crystalline silicon using a recently developed computational method for probing the thermodynamics of defects in solids. In this approach, the potential-energy landscape is sampled with lengthy molecular-dynamics simulations and repeated energy minimizations in order to build distribution functions that quantitatively describe the formation thermodynamics of a particular defect cluster. Using this method, a comprehensive picture for interstitial aggregation is proposed. In particular, we find that both vibrational and configuration entropic factors play important roles in determining self-interstitial cluster morphology. In addition to the expected role of temperature, we also find that applied (hydrostatic) pressure and the commensurate lattice strain greatly influence the resulting aggregation pathways. Interestingly, the effect of pressure appears to manifest not by altering the thermodynamics of individual defect configurations but rather by changing the overall energy landscape associated with the defect. These effects appear to be general and are predicted using multiple, well-tested, empirical interatomic potentials for silicon. Our results suggest that internal stress environments within a silicon wafer (e.g., created by ion implantation) could have profound effects on the observed self-interstitial cluster morphology.

DOI: 10.1103/PhysRevB.82.045206 PACS number(s): 61.72.jj, 61.72.Cc

I. INTRODUCTION

In an accompanying paper (Paper I),[1] it was shown that direct, large-scale molecular-dynamics (MD) simulations based on empirical interatomic potentials were able to spontaneously generate many of the complex self-interstitial cluster morphologies found in ion-implanted silicon samples. The various predicted structures were found to be in excellent structural agreement with microscopy observations and electronic-structure calculations.[2–7] Overall, the three different potentials employed, namely, the environment-dependent interatomic potential (EDIP),[8] Tersoff,[9] and Stillinger-Weber (SW),[10] all predicted consistent overall trends, leading to a qualitatively coherent picture for some aspects of self-interstitial clustering in silicon. In particular, it was found that cluster morphology is sensitively dependent on both the temperature and stress within the lattice. At high temperature (>0.75 Tm) and in the absence of stress, self-interstitial clusters tend to assume three-dimensional disordered structures that grow to large sizes (i.e., hundreds of interstitials) before suddenly transforming to planar defects aligned along the {111} directions. The {111} defects observed include rodlike defects (RLDs), partial dislocation loops, and perfect dislocation loops (PDLs); these structures have all been observed in experiment under various annealing conditions. The three-dimensional (3D) to two-dimensional (2D) transformation appears to be facile and proceeds rapidly without being subject to significant kinetic barriers. In the EDIP and SW simulations, lowering the temperature reduces the transition size but maintains the overall morphological evolution.

Under uniform tension for the EDIP and SW models, and at zero stress/low temperature for Tersoff, the {111} structures are no longer favored; instead, rodlike line interstitial defects (LIDs) and planar structures oriented along the {113} and {100} directions are found, with the {100} defects becoming increasingly favorable at higher temperatures. Although the {113} morphology is commonly observed in implanted silicon samples, the {100} planar defect is not, even though it has been found to be about as stable as the other morphologies. Moreover, {100} platelets are common in germanium[11] and carbon.[12,13] In aggregate, our results appear be in good agreement with many trends found in implantation experiments but also suggest that self-interstitial clustering may be somewhat complicated by the presence of multiple possible aggregation pathways that depend on both temperature and stress.

Formation thermodynamics for self-interstitial clusters—previous calculations

In this paper, we attempt to shed light on the various observations discussed in Paper I by studying in detail the thermodynamics of individual clusters. Previously reported analyses of self-interstitial cluster thermodynamics generally have focused on cluster energetics at zero temperature.[4–6,14–22] These studies have employed a broad range of theory to describe interatomic interactions, ranging from empirical potentials,[4,14,15] to tight binding,[16–18] to electronic density-functional theory (DFT).[5,6,20–23] While there are some discrepancies between the various studies regarding the precise values and ordering of the predicted formation energies, some general conclusions can be drawn. First, it is clear that on a per-interstitial basis, and in the limit of infinite size, the formation energy of all {111} planar defects is lower than either {100} or {113} defects.[4,5] Moreover, for clusters larger than some transition size, PDLs are the most stable of the {111}-oriented planar defects because of a lack of a stacking fault. Both of these results are consistent with the experimental observation that self-interstitial clusters eventually tend to coarsen into FDLs and then PDLs under most anneal-

ing conditions.[3,24–29] On the other hand, the absence of {100} planar defects in silicon wafer annealing experiments cannot be explained on the basis of simple energetics as these are found to possess formation energies that are very similar to the various configurations of {113} defects. For example, Goss[5] employed DFT within the local density approximation to compute the formation energies of infinite {100} and {113} defects, and found that the {100} defect was in fact slightly favored over the {113}. Chou *et al.*,[4] using the SW potential, find the reverse trend but again the difference is too small to explain the consistent lack of {100}-oriented planar structures in ion-implanted silicon wafers.

Using a combination of experimental observations, kinetic model regression to experimental data, and analytical models for defect energetics, the work by the ion implantation group at CNRS in Refs. 3, 27, and 30–35 built a comprehensive picture for the formation energies of the various self-interstitial cluster morphologies that is largely consistent with atomistic simulation results. Overall, a sequential process was described, which begins with the formation of small compact clusters of self-interstitials. These grow to form LIDs and {113} planar defects, the latter being the most energetically favorable up to cluster sizes of several hundred interstitials. At even larger sizes, the {113} defects are predicted to transform into the more favorable {111} planar defects; first FDLs are formed and then PDLs. No explicit consideration of {111} RLD defects was given in this energetic picture; all rodlike defects were assumed to be of the {113} type.

An additional important feature of self-interstitial cluster thermodynamics emerged in Ref. 2. Here, model regression to experimental measurements of dopant diffusion profiles strongly suggested that compact cluster formation energies in the size interval, $1<n_I<15$, were nonmonotonically evolving as a function of size. In particular, certain cluster sizes ($n_I=4$ and 8) were found to possess substantially lower formation energies per interstitial than neighboring sizes. This behavior has been qualitatively corroborated in some recent DFT studies[7] although the effect appeared to be significantly weaker in the DFT calculations than inferred from model regression, which shows very pronounced stability at $n_I=8$. Moreover, other DFT studies[6] did not find a similar effect and instead predicted a fairly monotonic decline in the per-interstitial formation energies in this size range.

In a recent publication,[36] we computed (using the empirical EDIP potential) the formation free energies of small interstitial clusters in the interval $1\leq n_I\leq 9$ and demonstrated that entropic contributions, particularly those arising from vibrational and configurational sources, can be significant. In fact, for the so-called Humble/Arai configuration[12,17,37] of the four-interstitial cluster [previously identified as the energetic ground state; see Fig. 1(a)], and the corresponding eight-interstitial configuration, the vibrational entropy was found to be substantially larger than that of other configurations at $n_I=4$ and 8. This entropic anomaly increases the relative stability of the four- and eight-intersitial clusters relative to other sizes. Moreover, the Humble/Arai configuration of the eight-interstitial cluster was also found to possess large configurational entropy that resulted from the numerous almost-degenerate ways in which two adjacent

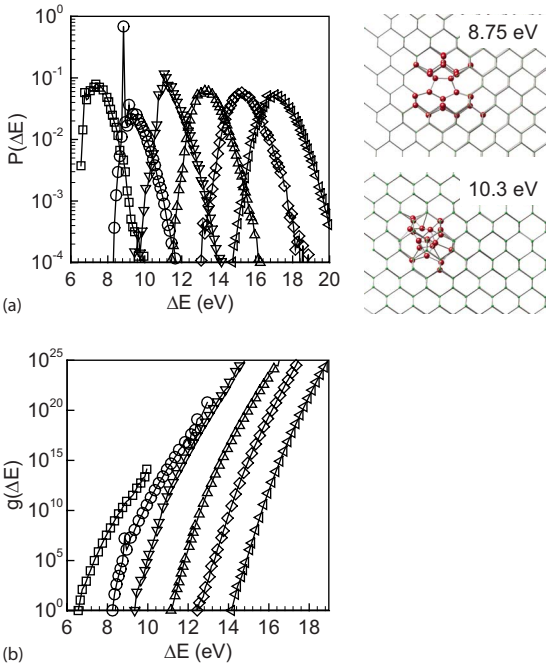

FIG. 1. (Color online) (a) Formation energy PDFs (at 1100 K) and (b) DOS for small interstitial clusters in the size range $3\leq n_I\leq 8$ computed with the EDIP potential. For both panels, squares represent $n_I=3$, circles $n_I=4$, gradients $n_I=5$, deltas $n_I=6$, diamonds $n_I=7$, and left triangles $n_I=8$. Insets in (a) show two configurations for the four-interstitial cluster; upper–Humble/Arai configuration, lower–extended, higher energy configuration.

Humble/Arai four-interstitial clusters could be placed relative to each other. Thus, while some special *energetic* stability was found at $n_I=4$ and 8, these two sizes were more strongly differentiated from the others when the *free energy* was considered.

The preceding observations are particularly relevant considering that the model regression in Ref. 2, which was based on comparisons of cluster concentrations measured as a function of time, generates estimates for effective formation *free* energies, rather than just energies. In other words, our previous results suggest that the reason why the model regression in Ref. 2 implied strong stability at $n_I=4$ and $n_I=8$ is at least partially due to the presence of entropic contributions at these sizes. We analyze this hypothesis further in the following sections using a more general thermodynamic framework, and also investigate how these features tie into the temperature and stress response of the aggregate morphology observed in Paper I.

The remainder of the paper is structured as follows. In the following section, we discuss the methodological details of a recently developed computational approach for analyzing the total (classical) free energy of defect clusters. In Sec. III, the results of calculations based on the EDIP are presented and discussed in detail. We place special emphasis on the analysis of entropic contributions, which have been largely ignored in the literature to date, but which can be extremely important in setting defect behavior at high temperature.[36,38–40] We also make mechanistic connections to the results obtained in the companion paper (Paper I).

Some of the calculations are repeated in Sec. IV using the formation enthalpy rather than the energy to define the distributions. In Sec. V, additional results obtained with other silicon empirical potentials are presented; these are primarily used to validate some of the principal conclusions drawn from the EDIP simulations. Finally, conclusions and a mechanistic picture for self-interstitial aggregation are presented in Sec. VI.

II. COMPUTATIONAL FRAMEWORK FOR SINGLE CLUSTER THERMODYNAMICS ANALYSIS

We have recently demonstrated that the total (classical) free energy of defect clusters in crystals can be modified substantially by configurational and vibrational entropy, particularly at elevated temperature.[38–42] Configurational entropy arises from the presence of numerous mechanically stable configurations that a defect cluster can assume within the lattice. Each of these configurations, α, (so called *inherent structures*) can be identified by a local energy minimum, V_α, in the multidimensional potential-energy landscape (PEL) that defines the overall system.[43,44] For solids and certain fluid states, the system can be assumed to spend the majority of its time in one of the local minima, only occasionally making excursions over the saddles separating the minima. Based on these ideas, as applied in previous work on supercooled liquids and glasses,[45,46] a direct computational approach for measuring the total (classical) free energy of a defect cluster has been developed; a brief discussion of the method is provided here and further details are given in Ref. 38.

In general, the total (classical) Helmholtz free energy of a system is given by $G=-k_BT\ln(Z)$, where Z is the canonical partition function. Assuming that the system of interest satisfies the assumptions described above, the partition function can be expressed as

$$Z=\exp\left(-\frac{G}{k_BT}\right)=\frac{1}{\Lambda^{3N}}\int g'(V_\alpha)\exp(-\beta V_\alpha)dV_\alpha, \quad (1)$$

where $\Lambda=(h^2/2\pi mk_BT)^{1/2}$ is the thermal de Broglie wavelength. The quantity $g'(V_\alpha)$ represents the density of states (DOS) or degeneracy of minima with an energy V_α and includes both configurational and vibrational states, i.e., $g'(V_\alpha)\equiv N_{vib}^{\alpha}g(V_\alpha)$, where $g(V_\alpha)$ is the configurational DOS and N_{vib}^{α} is the number of vibrational states in basins with energy V_α, i.e., $S_{vib}^{\alpha}=k\ln N_{vib}^{\alpha}$. Knowledge of the function $g'(V_\alpha)$ therefore directly leads to the free energy of the system; note that $g'(V_\alpha)$ is independent of temperature and can be used to compute free energies for all temperatures with application of Eq. (1).

In order to enumerate the local minima in the PEL, lengthy MD simulations of the system of interest (i.e., a bulk crystal containing a defect cluster) are performed. The local minima are found by periodically quenching the atomic coordinates generated by MD to the local minima; intervals of 100–200 time steps were used throughout the present work. Only configurations corresponding to connected clusters, as defined by the Stillinger criterion[43] are considered in the analysis. The occurrences are histogrammed into energy bins of width 0.1 eV. The resulting histogram is in fact the probability distribution function for the states of the system, i.e.,

$$p(V_\alpha)=g'(V_\alpha)\exp(-\beta V_\alpha) \quad (2)$$

from which the DOS can be obtained directly.

As shown in Ref. 38, the above procedure can be applied to systems with and without defects and the formation energy for a particular defect configuration is then given as $\Delta E_\alpha\equiv V_\alpha^d-(N_d/N_p)V^p$, where V^p is the energy of the perfect crystal, and N_p and N_d are the numbers of atoms in the perfect and defective systems, respectively. Finally, the total formation free energy of the defect is given by

$$\Delta G=-T\Delta S_{vib}^{ref}-k_BT\ln\int g(\Delta E)\exp[S_{vib}(\Delta E)/k_B]\times\exp(-\beta\Delta E_\alpha)d(\Delta E_\alpha), \quad (3)$$

where "ref" denotes some reference configuration for the defect and $\Delta S_{vib}^{ref}=S_d^{ref}-(N_d/N_P)S_p$. A reference configuration is only required for computing absolute free energies.[38]

MD simulations for PEL sampling were carried out in either the constant atom number, volume, and temperature (NVT) ensemble or constant atom number, pressure, and temperature (NPT) ensemble. In the former case, the system volume was chosen (using short NPT simulations) to provide the desired value of the hydrostatic pressure. Unless otherwise explicitly stated, the NVT ensemble was used as the default ensemble. Depending on the cluster size of interest ($1\leq n_I\leq 20$), simulation cells containing up to 8000 silicon lattice atoms were used. The fifth-order Gear predictor-corrector method[47] with time steps of 1.0–3.2 fs was used to integrate the particle trajectories; convergence of the simulation results with respect to the time step size was checked in each case using short test simulations.

III. THERMODYNAMIC ANALYSIS OF SINGLE SELF-INTERSTITIAL CLUSTERS-EDIP RESULTS

A. Probability distribution functions for small clusters at zero pressure

The probability distribution functions (PDFs) of cluster formation energies were computed for several small interstitial clusters ($3\leq n_I\leq 8$) at 1100 K and zero pressure using NVT simulations; these are shown in Fig. 1(a). It is important to emphasize once again, that the probability of observing any given configuration includes all entropic and energetic contributions, and that the total (classical) free energy of the defect cluster is proportional to the integral of the PDF. In general, the formation energy distributions are fairly broad, spanning several eV, and peak at some intermediate value demonstrating that at 1100 K, the most likely configurations are not necessarily those with the lowest formation energy. The general form of the PDFs is similar to that for vacancy clusters, which was discussed in detail in our previous work.[38]

The origin of the broad peak at intermediate formation energies in each case is best understood by considering Eqs.

(2) and (3); it is simply the point at which the exponential decay of the Boltzmann factor is balanced by the exponential growth of the degeneracy (i.e., the density of states, or DOS) as the formation energy increases. The exponential growth of degeneracy with increasing formation energy [see Fig. 1(b)] arises from the fact that higher formation energy configurations are increasingly spatially extended and therefore can generate more local minima in the potential energy landscape.[43,44] Several of the relaxed configurations for a given cluster were manually verified to correspond to well-defined local minima within the energy landscape. These configurations were perturbed by introducing small, random atomic displacements, and subsequently re-relaxed to the same local minimum. Obviously, sufficiently large disturbances were able to move the system away from a given configuration.

The PDF for the four-interstitial cluster in Fig. 1(a), however, exhibits an unusual feature—a sharp spike in the probability at $\Delta E = 8.75$ eV that dominates the entire distribution. In other words, under the conditions of 1100 K and zero stress, the equilibrium four-interstitial cluster spends over 80% of its time in configuration(s) with formation energy that lie in the interval $8.7 \leq \Delta E \leq 8.8$ eV. In fact, the single configuration that resides in this energy interval is the Humble/Arai configuration discussed in Paper I and Ref. 36; see the upper inset in Fig. 1(a). Other inherent structures for the four-interstitial cluster predicted by the EDIP potential are more disorganized; an example is shown in the lower inset in Fig. 1(a). Note that the anomalous spike corresponding to the Humble/Arai configuration in the four-interstitial probability distribution is not energetic in nature; neighboring configurations with almost the same formation energy are much less likely (by about a factor of 100) to be observed. Moreover, the EDIP potential actually identifies a few (low probability) configurations that have slightly lower formation energies than the Humble/Arai structure, a fact that is at odds with recent DFT results that predict this to be the energetic ground-state structure;[7] this issue will be addressed in more detail later.

One possible reason for the very high probability of observing the Humble/Arai configuration is that it possesses larger formation entropy (which may be vibrational and/or configurational in origin) than any other configuration of the four-interstitial cluster. In order to test this hypothesis, the vibrational formation entropy, defined as $S^f_{vib}(k_B) = (\Delta E - \Delta A)/T$, was computed within the quasi-harmonic approximation (QHA) (Ref. 48) for a large number of energy-minimized configurations for the four- and five-interstitial clusters; see Fig. 2. Two vacancy clusters ($n_V = 6$ and $n_V = 10$) also were considered for comparison. As shown in Fig. 2, all four clusters exhibit qualitatively similar behavior; overall the vibrational entropy of formation increases approximately linearly with formation energy, reflecting the tendency of more extended defects to produce a larger number of additional vibrational states into the crystal. The variability in the trend is somewhat larger for the self-interstitial clusters, which could arise because of their more complex morphologies. Closer inspection of the four-interstitial case, however, does confirm the suggestion that vibrational entropy is responsible for the special stability of the Humble/Arai configuration. The Humble/Arai configuration, denoted by the single large circle possesses vibrational entropy of formation that is at least $5-6k_B$ higher than neighboring configurations, which readily accounts for the 100-fold increase in probability for this particular configuration, i.e., $\exp(5) \sim O(10^2)$. In the remaining cases, no single configuration exhibits this anomaly and as a result the PDF varies relatively smoothly across the entire formation energy range.

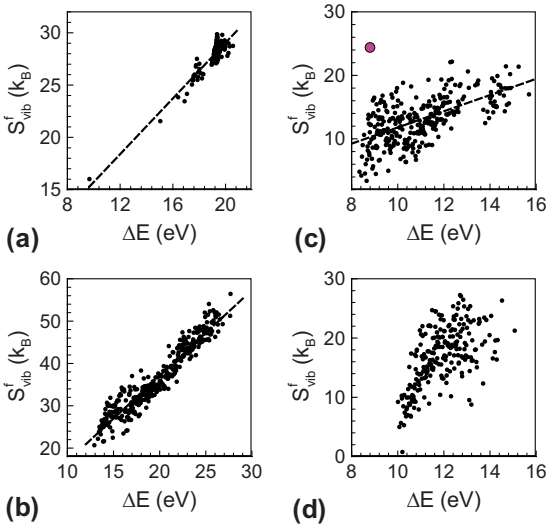

FIG. 2. (Color online) Vibrational entropy of formation for (a) six-vacancy, (b) ten-vacancy, (c) four-interstitial, and (d) five-interstitial clusters as a function of formation energy. Each symbol represents a QHA calculation for a single configuration of a given cluster. Large circle (purple) in (c) represents the Humble/Arai configuration. Dashed lines are guides only.

It is notable that the eight-interstitial cluster, which can assume configurations corresponding to two adjacent Humble/Arai building blocks, does not exhibit the sharp spike structure in its PDF [see Fig. 1(a)], even though these configurations also are expected to possess large vibrational entropy. The reason for this apparent anomaly will be discussed in the following section. The entropic nature of the stabilization of the Humble/Arai configuration of the four-interstitial cluster would suggest that it is insensitive to the effect of temperature. Indeed, the probability spike in the four-interstitial PDF persists as the temperature is increased, as shown in Fig. 3.

Although the overall PDF for the four-interstitial cluster shifts to the right with increasing temperature, the Humble/Arai spike remains due to the increasing importance of its high vibrational entropy of formation. As a result, it is expected that the Humble/Arai configuration should play an important role in self-interstitial clustering kinetics, even at the elevated temperatures typically employed in damage annealing. This conclusion can be contrasted starkly with the more common case of energetic stabilization of "magic" cluster sizes, such as for vacancy clusters.[49,50] In the energetic stabilization case, clusters of particular sizes are favored relative to others at low temperature because certain configurations minimize the formation energy (e.g., by the minimization of dangling bonds). However, at elevated temperature, this effect is obscured by entropic contributions and

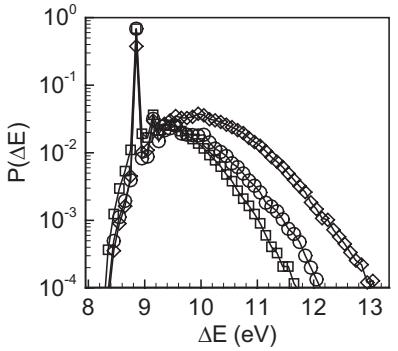

FIG. 3. Four-interstitial cluster PDFs as a function of temperature (and zero pressure). Squares–1100 K, circles–1200 K, and diamonds–1300 K.

the formation free energy per vacancy is found to decrease almost monotonically with cluster size. Stated another way, magic sizes of silicon vacancy clusters (and any other energetically stabilized cluster) are not important at the high temperatures relevant to crystal growth and wafer annealing, whereas in the case of self-interstitials, such "magicness" appears to be largely entropically driven and therefore can be relevant at any temperature. We conclude this discussion by suggesting the interesting possibility that fine structure within a PDF for a given cluster size, such as that observed for the four-interstitial cluster, may be used as a marker for identifying cluster magicness. The fact that the overall PDF is strongly influenced by this single, low free-energy configuration indicates that the overall formation free energy of the four-interstitial is likely to be lower than that of neighboring cluster sizes on a per-interstitial basis.

B. Effect of hydrostatic pressure on the thermodynamics of small interstitial clusters

While the entropic stabilization of the four-interstitial cluster renders it relatively insensitive to temperature, it is surprisingly sensitive to pressure (or equivalently, lattice strain). Shown in Fig. 4(a) are the area-normalized PDFs at 1100K for the four-interstitial cluster at zero pressure, +3 GPa hydrostatic compression (approx. −1% compressive strain), and −3 GPa hydrostatic tension (approx. 1% tensile strain). The peak related to the Humble/Arai configuration is seen to become even more pronounced under tension and is now predicted to be the absolute lowest energy structure, i.e., the few (low-probability) local minima in the PEL to the left of the Humble/Arai peak observed at zero pressure disappear under applied tension. Conversely, under compression, the Humble/Arai peak completely disappears and the four-interstitial PDF becomes smoothly varying as for the other cluster sizes shown in Fig. 1(a).

At first glance, it would seem that these results indicate that the formation thermodynamics of the Humble/Arai structure for the four-interstitial cluster depend strongly on hydrostatic pressure. The formation energy, vibrational entropy, and total Helmholtz free energy were computed for the Humble/Arai structure as a function of pressure and are shown in the inset of Fig. 4(a). Clearly, the formation thermodynamics of the Humble/Arai configuration are essentially independent of hydrostatic pressure. The slight apparent increase in the formation entropy under compression is mostly a result of scatter in the data, and in any case, would predict that the Humble/Arai structure is increasingly dominant under compression, i.e., opposite to the trend in Fig. 4(a).

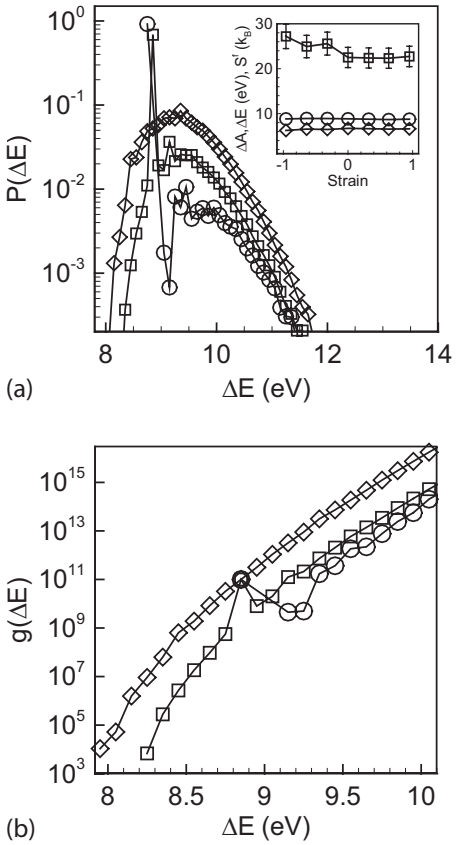

FIG. 4. (a) PDF for the four-interstitial cluster as a function of hydrostatic pressure: squares—zero pressure; circles—−3 GPa pressure (1% tensile strain); and diamonds—+3 GPa pressure (1% compression). Inset: formation thermodynamics for the four-interstitial Humble/Arai configuration as a function of strain (diamonds—free energy, circles—energy, and squares—vibrational entropy). (b) Four-interstitial DOS as a function of pressure anchored to the Humble/Arai configuration (see text): squares—zero pressure; circles—−3 GPa applied pressure (1% tension); and diamonds—+3 GPa applied pressure (1% compression).

The interesting effect of stress on the stability of the Humble/Arai configuration observed here instead arises from the density-of-states function for the four-interstitial cluster, $g'(\Delta E)$ shown in Fig. 4(b), where $g'(\Delta E)=p(\Delta E)\exp(\beta\Delta E)$. The three curves shown represent the DOS at each of the three stress conditions and have been anchored to each other on the basis of the formation energy interval containing the Humble/Arai structure. Assuming that the formation energy bin containing the Humble/Arai configuration (centered at $\Delta E=8.75$ eV) is entirely comprised of that single state, the DOS functions for the three curves must be equal at that value of formation energy. Further assuming that the configurational degeneracy of the Humble/Arai configuration is O(1) based on the D_{2d} symmetry of the structure, the total

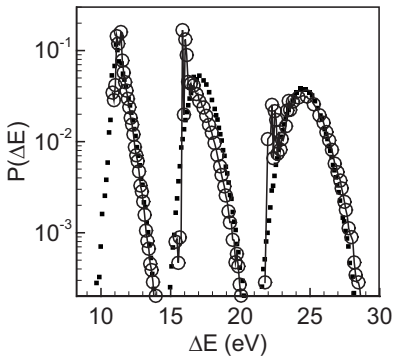

FIG. 5. Effect of hydrostatic pressure on the probability distribution functions for the five-, eight-, and 12-interstitial clusters (shown left to right, respectively). Filled squares denote zero stress and open circles denote −3 GPa applied pressure (approx. 1% tensile strain).

number of states in that energy interval must arise entirely from vibrational contributions, i.e., $g'(\Delta E) \sim N_{vib}$, where $N_{vib} = \exp(S_{vib}/k_B) \sim 1 \times 10^{11}$ and $(S_{vib} \sim 25k_B)$ for the Humble/Arai configuration. These considerations allow us to anchor the three DOS curves to absolute values and make quantitative comparisons between them. Further details regarding the anchoring of DOS curves are provided in Ref. 38.

Comparison of the three DOS functions in Fig. 4(b) shows clearly that the overall density of states increases with increasing hydrostatic pressure. The apparent decreased stability of the Humble/Arai structure under compression therefore arises because additional states (i.e., local minima in the PEL) are introduced by the compression, reducing the probability of observing that particular configuration. Conversely, tension appears to lower the overall density of states and increases the dominance of the Humble/Arai configuration relative to all others. Interestingly, all local minima with energies below that of the Humble/Arai structure become mechanically unstable under −3 GPa hydrostatic tension (approx. 1% tensile strain) and the Humble/Arai structure now is predicted to the be ground-state structure. Thus, we find that it is not the formation thermodynamics of the Humble/Arai configuration that depend strongly on pressure but rather the density of all other configurations that collectively compete with this special configuration.

The mechanism by which the overall DOS is affected by lattice stress is not immediately obvious. It is plausible to suppose that as atoms are brought into closer contact by compression, increasing the number of neighbors per particle, the PEL predicted by the EDIP interatomic potential becomes more complex (i.e., rougher) and the number of local minima in a given energy interval increases. Whether this is generally true for other interatomic potentials such as Tersoff will be addressed in Sec. V.

The effect of hydrostatic pressure on other cluster sizes $(n_I = 5, 8, 12)$ is shown in Fig. 5 for comparison. For each cluster size the formation energy PDF is shown for zero stress (small filled squares) and at −3 GPa tensile hydrostatic pressure (large open circles); all PDFs are normalized to unit area. For the eight-interstitial and 12-interstitial clusters, a significant change is observed in which a spike similar to that observed for the four-interstitial case appears under tension. By contrast, the five-interstitial distribution is essentially unresponsive to stress. Once again, the effect of tension on the eight-interstitial and 12-interstitial PDFs arises from a reduction in the overall DOS, thereby increasing the significance of a few cluster configurations that possess increased stability relative to the rest within the distribution. The eight- and 12-interstitial clusters are expected to possess similar behavior to that of the four-interstitial cluster because they are able to assume configurations that are comprised of integer multiples of the Humble/Arai building block. Because these special structures are absent in the five-interstitial case, no effect is observed on the overall PDF. Thus, even though the overall density of states may be reduced by tensile lattice stress, the DOS is reduced evenly across the energy spectrum and the areal normalization maps them onto each other.

Examples of the special configurations for the eight-interstitial cluster that become dominant under lattice tension are shown in Fig. 6, along with their assignments to various locations in the eight-interstitial PDF at −3 GPa hydrostatic tension. The two peaks located at formation energies $\Delta E = 15.86$ eV and $\Delta E = 16.05$ eV, labeled by (i) and (ii) in Fig. 6, respectively, correspond to configurations comprised of

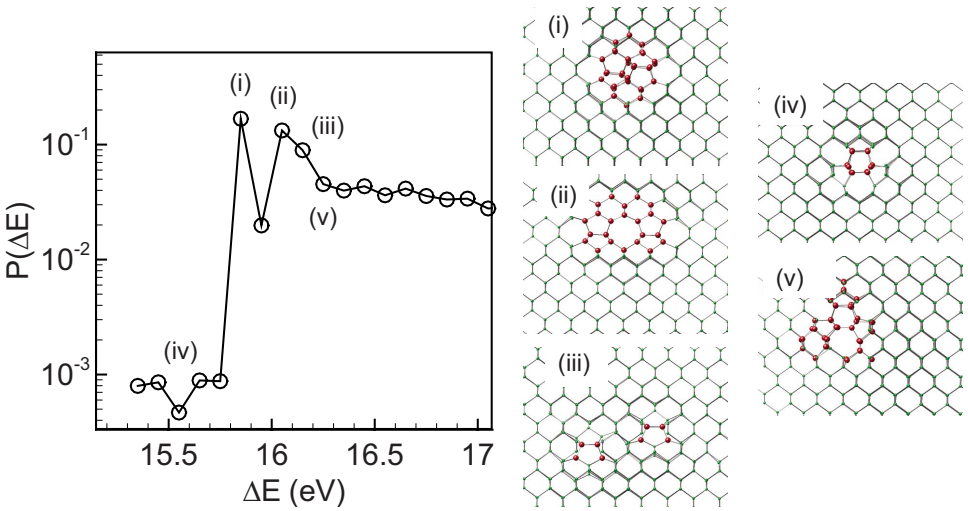

FIG. 6. (Color online) Formation energy PDF for the eight-interstitial cluster at 1100 K and −3 GPa applied pressure (approx. 1% tensile strain) highlighting the distribution at low values of formation energy. The eight-interstitial configurations that correspond to the various numbered locations on the PDF are shown in the insets on the right-hand side of the figure.

two adjacent Humble/Arai four-interstitial blocks (see insets). Another such configuration (iii) appears at a formation energy $\Delta E = 16.23$ eV. Note that the configuration (ii) is essentially a very small {100} defect showing clearly the alternating five- and eight-membered ring structure found in our parallel molecular dynamics (PMD) simulations in Paper I and also in previous work.[36] Each of these three configurations is stabilized by the high vibrational entropy associated with the Humble/Arai structure, which explains their high probability of being observed in the PDF for the eight-interstitial cluster. Collectively, they also suggest yet another source of entropy which is configurational in nature. As discussed in Ref. 36, there are in fact a large number of possible (and nearly degenerate) ways to arrange two Humble/Arai four-interstitial building blocks to form a cluster of size 8. Based on a very rough estimation, this configurational entropic source can additionally lower the free energy of the eight-interstitial cluster by a few tenths of an electron volt per interstitial.[36]

Configurations labeled (iv) ($\Delta E = 15.56$ eV) and (v) ($\Delta E = 16.26$ eV) in Fig. 6 represent a fundamentally different arrangement of the eight interstitials within the cluster. Both of these configurations are comprised of a single row of interstitials aligned in the {110} direction and are in fact LIDs that have not yet fully reconstructed.[51] In other words, structures (iv) and (v) are building blocks for planar {113} defects. Configuration (v) is higher in energy due to rearrangement in the atomic position surrounding the interstitial row but is otherwise essentially the same structure as (iv). Although the LID configuration is approximately energetically degenerate to the Humble/Arai configurations, they appear at substantially lower probabilities; in fact, structure (iv), although lowest in formation energy, possesses very low probability. The difference in probability of observing the {100} precursors [i.e., (i), (ii), or (iii)] versus the {113} precursors [i.e., (iv) or (v)] is entirely attributable to the special vibrational entropy of configurations based on the Humble/Arai motif. As shown previously in Ref. 36, configuration (i) possesses up to $2k_B$ of additional vibrational entropy per interstitial relative to configuration (iv), which is amply sufficient to explain the almost 1000-fold increase in probability associated with the former structure relative to the latter. Similar vibrational entropy enhancement is attributable to the various different arrangements of two Humble/Arai building blocks. These arguments are expected also to apply to the case of 12-interstitial (and larger) clusters, which simply include additional Humble/Arai building blocks.

The interplay between energetic and entropic stabilization of the {100} and {113} precursors suggests an explanation for some of the observations in Paper I. There, it was found that {100} and {113} were generally found together but that {100} defects were more likely to form at higher temperatures and {113} were only found at lower simulation temperature. The above considerations indicate that in order to observe these special structures, the overall density of states must be low enough to allow them to be dominant; for the EDIP potential at least, this is accomplished by presenting a tensile environment within the lattice. The propensity for forming {100} defects at higher temperatures arises because of the additional vibrational entropy associated with the Humble/Arai motif. On the other hand, at lower temperatures, the lower formation energy of the {113} precursor could dominate. The one thing our results do not appear to resolve is why the {100} planar defects are not more frequently observed in experiment—these structures are both energetically and entropically favorable.

Finally, we note that as the cluster size increases, the overall density of states should increase, reducing the dominance of the {100} and {113} precursors relative to the disordered configurations. This is in fact why the eight-interstitial cluster requires tension to present structure in the DOS while the four-intersitial cluster does not. As shown previously in Fig. 5, the spikes in the PDF corresponding to {113} and {100} precursors for the 12-interstitial cluster are seen to be relatively small compared to the remainder of the distribution at −3 GPa hydrostatic tension. In other words, as the cluster size increases the possible dominance of single configurations becomes increasingly unlikely. However, as the cluster size increases, the morphology of the cluster is likely to already be well-established and further growth would be directed within the {100} or {113} motifs.

IV. CALCULATION OF FORMATION ENTHALPY PDFs

In the preceding sections, NVT MD calculations were employed to compute probability distribution functions for cluster formation energies. Although the system volume in each case was chosen to correspond to a desired applied pressure, the pressure is generally not constant in an NVT simulation unless the formation volume[52] of all cluster configurations, defined as[52]

$$\Delta V_\alpha = V_\alpha^d - (N_d/N_p)V^p, \tag{4}$$

is equal. In Eq. (4), the "d" and "p" superscripts denote the defective and perfect systems, respectively, which are both held at the same pressure (or more generally, stress). For the general case where the formation volumes are variable, configurations that have large formation volume magnitudes may be subject to tension or compression, altering their formation *enthalpies*; this effect would not be captured in the formation *energy* distributions calculated in the prior sections. Moreover, the energy minimization for each configuration also was performed at constant volume, which generally leads to the generation of additional tension in the final structures because the average lattice parameter is larger at high temperature than it is at zero temperature.[53,54]

In order to assess whether these assumptions materially affect the results presented in the previous sections, we repeated the calculations of the PDF for the four-interstitial cluster at 1100 K within the NPT ensemble. In these calculations, all energy minimizations also were performed at constant pressure (i.e., the simulation box was allowed to change size during energy minimization) in order to ensure that the final formation enthalpy was defined at the intended pressure. The LAMMPS code[55] with our implementation of the EDIP potential was used for these calculations. Shown in Fig. 7 are the formation energy PDFs for the four-interstitial cluster at zero pressure using both the NVT and NPT ensembles. The excellent agreement between the two simula-

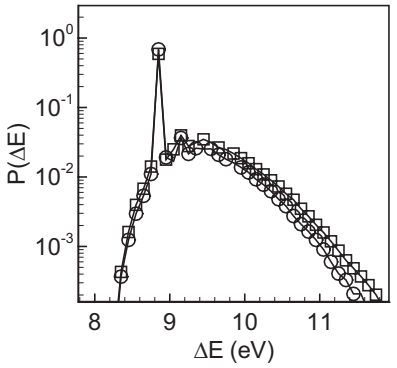

FIG. 7. Formation energy PDF for the four-interstitial cluster at 1100 K and zero applied stress/strain: squares—NPT MD with constant-pressure energy minimization and circles—NVT MD with constant-volume energy minimization.

tions suggests that the effect of induced tension during energy minimization at constant volume is negligible and also that the formation volume change across the PDF is not large. The slight deviation of the two distributions at higher energies may be the result of bias introduced by the constant volume calculations but the absolute value of the probabilities are small in this region.

Next, formation energy PDFs were computed at three different applied pressures (−3 GPa, 0, and +3 GPa) using the NPT ensemble; see Fig. 8. The location of the peak related to the Humble/Arai configuration is clearly unaffected by the applied pressure although the overall distributions are modified by the introduction (or removal) of states as discussed earlier in Sec. III B. Again, these results are in excellent agreement with those obtained using the constant volume calculations in Sec. III B.

We note here that recent DFT calculations[22] appear, in contrast to our present findings, to demonstrate very significant dependence of the formation energy on hydrostatic strain for the Humble/Arai configuration of the four-interstitial (at zero temperature). The apparent discrepancy can be resolved by noting that the formation properties computed in Ref. 22 were defined so that the reference and defective simulation cells were held at the same far-field lattice parameter, rather than the same applied stress.

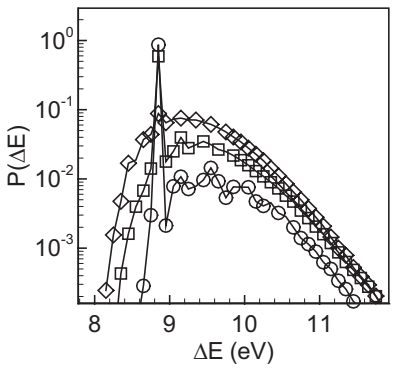

FIG. 8. Formation energy PDFs for the four-interstitial cluster at 1100 K as a function of applied pressure (NPT MD): squares—zero pressure, circles—−3 GPa (approx 1% tensile strain), and diamonds—+3 GPa (approx. 1% compressive strain).

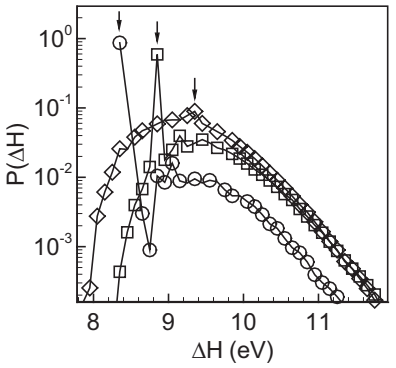

FIG. 9. Formation enthalpy PDFs (NPT MD) for the four-interstitial cluster at 1100 K as a function of applied pressure: squares—zero pressure, circles—−3 GPa (approx 1% tensile strain), and diamonds—+3 GPa (approx. 1% compressive strain). The arrows indicate the location of the enthalpy bin containing the Humble/Arai configuration.

Although the formation energy appears to be unaffected by applied pressure, it is the formation enthalpy that is most relevant under finite applied stress. The formation enthalpy distributions at three different pressures were computed using our NPT framework at 1100 K. Here, the formation enthalpies for a particular configuration, α, like the corresponding formation energies, were computed based on the relationship

$$\Delta H_\alpha(P) \equiv H_\alpha^d(P) - (N_d/N_p)H^p(P), \tag{5}$$

where the pressure dependence of the enthalpy is made explicit.

As shown in Fig. 9, the formation enthalpy of the Humble/Arai configuration (denoted by arrows) shifts by about 0.5 eV in either direction when 3GPa of pressure is applied (compressive or tensile). Since the formation energy is constant, this shift is entirely attributable to the PV contribution arising from the nonzero formation volume of the defect. For the Humble/Arai configuration, the formation volume is approximately 20 $Å^3$, which corresponds approximately to the volume of a single lattice atom. In other words, the Humble/Arai configuration of the four-interstitial defect occupies about the same total volume as five perfect silicon atoms [see Eq. (4)].

A plot of the formation volume as a function of formation energy for numerous configurations of the four-interstitial cluster is shown in Fig. 10; these values were computed at 1100 K and zero pressure. Although the formation volumes tend to increase with formation energy, they are generally small across the range of formation energies accessed in the calculation. Note that many configurations, particularly those with low energies of formation, exhibit negative formation volume, i.e., they occupy less space than the perfect crystal on a per-atom basis. This is not unexpected given the relative openness of the diamond lattice, as compared to close-packed lattices such as fcc. A consequence of these results is that the formation enthalpy of the various four-interstitial configurations, including the Humble/Arai one, are relatively weakly dependent on applied stress.

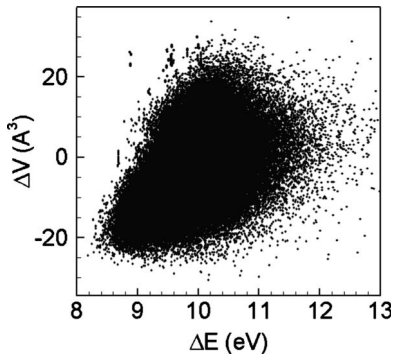

FIG. 10. Formation volume as a function of formation energy for four-interstitial configurations at zero pressure.

V. TERSOFF POTENTIAL RESULTS

In Paper I it was shown that the overall self-interstitial cluster morphological evolutions predicted by EDIP, Tersoff, and to a lesser extent SW, were essentially consistent. The primary discrepancy that was noted between the EDIP and Tersoff results was that Tersoff appeared to favor the formation of {100} and some {113} defects at zero applied stress and low temperature while EDIP requires applied tension before stabilizing any {113} defect precursors (i.e., LIDS). Here we compare the formation energy probability distributions for the four- and eight-interstitial clusters in order to explain this difference.

The Tersoff-generated formation energy PDFs for the four- and eight-interstitial clusters at 1900 K are shown in Fig. 11. Both 0 and +3 GPa compressive pressure (1% compressive strain) cases are considered. In the four-interstitial case, the compressive stress does not appear to substantially reduce the probability of observing the Humble/Arai configuration ($\Delta E=8$ eV) although small shifts in the probabilities of higher energy configurations are observed. This is in contrast to the EDIP case [Fig. 4(a)], where +3 GPa hydrostatic compression led to the disappearance of the Humble/Arai peak in the PDF. On the other hand, the eight-interstitial cluster behavior is qualitatively similar to that of the EDIP

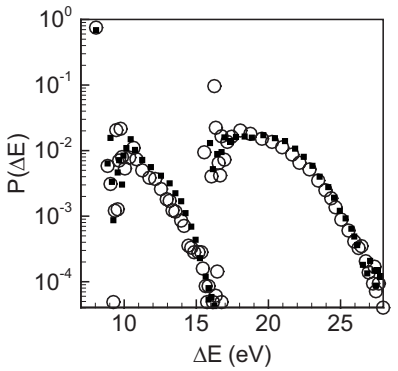

FIG. 11. Tersoff generated (NVT MD) formation energy PDFs for the four-interstitial (left) and eight-interstitial (right) clusters at 1900 K as a function of applied pressure: open circles—zero pressure and small filled squares—+3 GPa applied pressure (approx, 1% compressive strain).

case, whereby the peaks associated with Humble/Arai configurations and ⟨110⟩-oriented interstitial chains (LID precursors) are substantially reduced by the application of compression.

Overall, the effect of stress on the density of states observed in the EDIP case is reproduced in the Tersoff calculations indicating that this is a general phenomenon. However, the dominance of the Humble/Arai configuration for the four-interstitial cluster in the Tersoff model appears to be more pronounced than that in EDIP, which explains the increased propensity to observe {100} and {113} related structures in the 1900 K Tersoff simulations reported in Paper I. These observations suggest a qualitative difference in the potential-energy landscape roughness predicted by the two models although a more quantitative analysis of this statement would require more detailed calculations that are beyond the scope of the present study. In other words, the EDIP potential landscape associated with self-interstitial clusters may be rougher that that of the Tersoff one (i.e., containing a larger number of local minima), thereby making it more difficult for a single configuration to dominate even if it possesses uniquely favorable properties such as high vibrational entropy. In both cases, compression appears to increase the roughness of the landscape, eventually drowning out peaks associated with special structures.

VI. A MECHANISTIC SUMMARY AND CONCLUSIONS

The results presented here and in Paper I suggest an intriguing mechanistic picture for morphology selection in self-interstitial clustering in which lattice stress, and its effect on entropy rather than energy, potentially plays an important role. We identify two broad situations that are largely consistent across both the EDIP and Tersoff potentials.

A. Low temperature and/or tensile stress

Under these conditions, special configurations of certain cluster sizes such as $n_I=4,8,12$ are favored over other possible rearrangements by a combination of low formation energy and large vibrational entropy. For $n_I=8$ and 12, two main types of distinguishable configurations are possible, which are directly related to the formation of {113} and {100} planar defects. The former is an elongated chainlike structure aligned along the ⟨110⟩ directions and has been discussed at length in previous experimental and theoretical studies. The latter is much less well studied within the silicon literature because of the scarcity of {100} planar defect observations in ion-implanted silicon although these are commonly observed in diamond and germanium.[11,12] This configuration is particularly favored by its high vibrational entropy because it is comprised of an integer number of Humble/Arai building blocks. The growth of both types of structures leads to the eventual formation of {113} and {100} planar defects, both of which were directly observed in the large-scale simulations presented in Sec. III. It is not possible to extend our simulations to the point at which {113} defects evolve by unfaulting into lower energy {111} defects but previous work shows that this transition is expected at around $n_I=500$.[3,27,56]

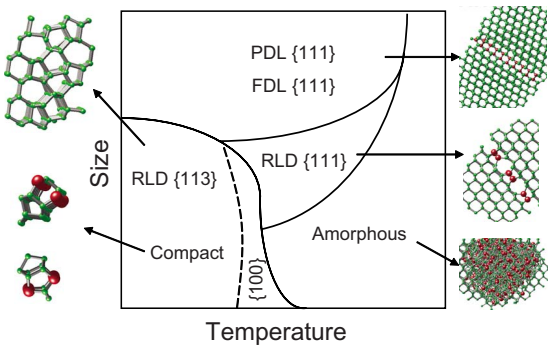

FIG. 12. (Color online) Evolution map for self-interstitial aggregation as a function of cluster size and temperature. In most cases, the effect of hydrostatic pressure is qualitatively similar to increasing the temperature.

B. Higher temperatures with no compression

Here, the overall density of states associated with interstitial clusters at most sizes (except $n_I=4$) is sufficiently large so as to "drown out" the special configurations that lead to the {100} and {113} planar defects. As a result, most small clusters assume three-dimensional amorphous configurations up to a certain (temperature and pressure dependent) critical size at which point they collapse into {111}-oriented planar defects of various types including RLDs, FDLs, and PDLs, all of which have been observed experimentally. In this growth mode, the transition to {111} defects is much earlier than that associated with the {113}-{111} transition suggested in Refs. 3, 27, and 56, and {113} defects are never formed. However, note that even at zero stress, {100} defects are still observed because of the large vibrational entropy associated with the Humble/Arai configuration.

Our results therefore suggest that applied stress can dramatically alter the pathway by which self-interstitials aggregate to form the various types of cluster morphologies observed in the literature. A key aspect of this mechanism is that the stress acts by modifying the overall density of states distribution of formation energies associated with a cluster, rather than by strongly modifying the formation thermodynamics of a particular cluster structure. Thus, although the particular cluster configurations responsible for {113} and {100} motif formation are entropically stabilized relative to other configurations, this stabilization can become overwhelmed by the large number of other possible (usually higher energy) configurations. Unfortunately, our results do not explain the apparent dearth of {100}-oriented defects in damaged, interstitial-rich silicon; in agreement with previous calculations, these are found to be both energetically and now, also entropically, favorable.

A temperature-size phase diagram for the morphology of self-interstitial clusters is shown in Fig. 12 that summarizes much of the results obtained in the present work. Very small interstitial clusters assume compact morphologies that exhibit special stability at certain sizes. Importantly, each cluster is associated with numerous possible configurations that collectively increase the configuration entropy of the defect; as the temperature is increased, this effect becomes increasingly significant. At certain cluster sizes, one or more special configurations are dominant because of their large vibrational entropy; this effect serves to lower the overall formation free energy of these sizes. The evolution of cluster morphology with size depends strongly on both temperature and stress as shown in Fig. 12. Interestingly, the effects of both temperature and stress are manifested through entropic means. The latter, in particular, is worth emphasizing; stress appears to play its role by altering the roughness of the potential-energy landscape associated with interstitial defects. Compression (and elevated temperature) appears to increase landscape roughness, reducing the influence of the special configurations that lead to the growth of {113} and {100} rodlike and planar structures at larger sizes. As a result, we identify conditions of temperature and stress that lead to an unexpected direct transition between amorphous three-dimensional configurations and planar {111} planar loops at rather small cluster sizes.

The speculation on the possible role of stress/strain in self-interstitial aggregation will require further study. Although hydrostatic stress is generally not engineered into the systems of interest, the implantation process itself can generate complex and transiently varying stress fields that depend in a complex fashion on the implant dose, type, and energy.[29,57,58] Future work in this area might be required to determine whether the stresses arising from implantation and damage annealing can influence the clustering process. On the other hand, biaxial and uniaxial stress fields are more common and further work will be required to characterize the effect of these fields on self-interstitial clustering. Recent DFT calculations show that in some cases the differences may be important and may lead to additional heterogeneities in the cluster distribution.[22]

Finally, we note once again that the preceding conclusions depend substantially on the validity of the empirical EDIP and Tersoff potentials. It should be emphasized that all defect structures that were generated spontaneously in the simulations in Paper I are largely consistent with structures that have been verified by high-resolution transmission electron microscopy as well as DFT calculations. This includes the small compact clusters (e.g., $n_I=4,8$), the elongated, rodlike clusters ($n_I=8,12$), and the various planar structures formed in the large-scale aggregation simulations. Comparing the formation energies of small, compact clusters to DFT estimates in Ref. 7 further demonstrate that these empirical potentials are able to at least qualitatively capture much of the general picture associated with self-interstitial clustering, if not the precise thermodynamic properties.

ACKNOWLEDGMENT

We gratefully acknowledge financial support from the National Science Foundation (Grants No. CTS01-34418 and No. CBET-0730971).

*Corresponding author; talid@seas.upenn.edu

[1] S. S. Kapur and T. Sinno, preceding paper, Phys. Rev. B **82**, 045205 (2010).
[2] N. E. B. Cowern, G. Mannino, P. A. Stolk, F. Roozeboom, H. G. A. Huizing, J. G. M. van Berkum, F. Cristiano, A. Claverie, and M. Jaraiz, Phys. Rev. Lett. **82**, 4460 (1999).
[3] A. Claverie, B. Colombeau, B. De Mauduit, C. Bonafos, X. Hebras, G. Ben Assayag, and F. Cristiano, Appl. Phys. A **76**, 1025 (2003).
[4] C. T. Chou, D. J. H. Cockayne, J. Zou, P. Kringhoj, and C. Jagadish, Phys. Rev. B **52**, 17223 (1995).
[5] J. P. Goss, T. A. G. Eberlein, R. Jones, N. Pinho, A. T. Blumenau, T. Frauenheim, P. R. Briddon, and S. Öberg, J. Phys.: Condens. Matter **14**, 12843 (2002).
[6] J. Kim, F. Kirchhoff, J. W. Wilkins, and F. S. Khan, Phys. Rev. Lett. **84**, 503 (2000).
[7] S. Lee and G. S. Hwang, Phys. Rev. B **77**, 085210 (2008).
[8] M. Z. Bazant, E. Kaxiras, and J. F. Justo, Phys. Rev. B **56**, 8542 (1997).
[9] J. Tersoff, Phys. Rev. B **38**, 9902 (1988).
[10] F. H. Stillinger and T. A. Weber, Phys. Rev. B **31**, 5262 (1985).
[11] S. Muto and S. Takeda, Philos. Mag. Lett. **72**, 99 (1995).
[12] P. Humble, Proc. R. Soc. London **381**, 65 (1982).
[13] J. P. Goss, B. J. Coomer, R. Jones, C. J. Fall, P. R. Briddon, and S. Oberg, Phys. Rev. B **67**, 165208 (2003).
[14] M. Kohyama and S. Takeda, Phys. Rev. B **46**, 12305 (1992).
[15] S. Birner, J. Kim, D. A. Richie, J. W. Wilkins, A. F. Voter, and T. Lenosky, Solid State Commun. **120**, 279 (2001).
[16] M. Kohyama and S. Takeda, Phys. Rev. B **51**, 13111 (1995).
[17] N. Arai, S. Takeda, and M. Kohyama, Phys. Rev. Lett. **78**, 4265 (1997).
[18] J. N. Kim, J. W. Wilkins, F. S. Khan, and A. Canning, Phys. Rev. B **55**, 16186 (1997).
[19] A. Bongiorno, L. Colombo, F. Cargnoni, C. Gatti, and M. Rosati, Europhys. Lett. **50**, 608 (2000).
[20] M. Kohyama and S. Takeda, Phys. Rev. B **60**, 8075 (1999).
[21] J. Kim, F. Kirchhoff, W. G. Aulbur, J. W. Wilkins, F. S. Khan, and G. Kresse, Phys. Rev. Lett. **83**, 1990 (1999).
[22] R. J. Bondi, S. Lee, and G. S. Hwang, Phys. Rev. B **80**, 125202 (2009).
[23] R. J. Bondi, S. Lee, and G. S. Hwang, Phys. Rev. B **79**, 104106 (2009).
[24] G. Z. Pan, K. N. Tu, and S. Prussin, Appl. Phys. Lett. **71**, 659 (1997).
[25] G. Z. Pan, K. N. Tu, and A. Prussin, J. Appl. Phys. **81**, 78 (1997).
[26] G. Z. Pan and K. N. Tu, J. Appl. Phys. **82**, 601 (1997).
[27] F. Cristiano, N. Cherkashin, X. Hebras, P. Calvo, Y. Lamrani, E. Scheid, B. de Mauduit, B. Colombeau, W. Lerch, S. Paul, and A. Claverie, Nucl. Instrum. Methods Phys. Res. B **216**, 46 (2004).
[28] J. H. Li and K. S. Jones, Appl. Phys. Lett. **73**, 3748 (1998).
[29] K. S. Jones, J. Liu, L. Zhang, V. Krishnamoorthy, and R. T. DeHoff, Nucl. Instrum. Methods Phys. Res. B **106**, 227 (1995).
[30] F. Cristiano, B. Colombeau, C. Bonafos, A. Altibelli, G. Benassayag, and A. Claverie, Solid State Phenom. **82-84**, 201 (2002).
[31] A. Claverie, L. Laanab, C. Bonafos, C. Bergaud, A. Martinez, and D. Mathiot, Nucl. Instrum. Methods Phys. Res. B **96**, 202 (1995).
[32] A. Claverie, L. F. Giles, M. Omri, B. de Mauduit, G. Ben Assayag, and D. Mathiot, Nucl. Instrum. Methods Phys. Res. B **147**, 1 (1999).
[33] A. Claverie, B. Colombeau, F. Cristiano, A. Altibelli, and C. Bonafos, Nucl. Instrum. Methods Phys. Res. B **186**, 281 (2002).
[34] S. Boninelli, N. Cherkashin, A. Claverie, and F. Cristiano, Appl. Phys. Lett. **89**, 161904 (2006).
[35] S. Boninelli, N. Cherkashin, A. Claverie, and F. Cristiano, Nucl. Instrum. Methods Phys. Res. B **253**, 80 (2006).
[36] S. S. Kapur and T. Sinno, Appl. Phys. Lett. **93**, 221911 (2008).
[37] B. J. Coomer, J. P. Goss, R. Jones, S. Oberg, and P. R. Briddon, J. Phys.: Condens. Matter **13**, L1 (2001).
[38] S. S. Kapur, M. Prasad, J. C. Crocker, and T. Sinno, Phys. Rev. B **72**, 014119 (2005).
[39] J. G. Dai, J. M. Kanter, S. S. Kapur, W. D. Seider, and T. Sinno, Phys. Rev. B **72**, 134102 (2005).
[40] J. Dai, W. D. Seider, and T. Sinno, Mol. Simul. **32**, 305 (2006).
[41] M. Prasad and T. Sinno, Phys. Rev. B **68**, 045207 (2003).
[42] T. A. Frewen, S. S. Kapur, W. Haeckl, W. von Ammon, and T. Sinno, J. Cryst. Growth **279**, 258 (2005).
[43] F. H. Stillinger, J. Chem. Phys. **38**, 1486 (1963).
[44] M. Goldstein J. Chem. Phys. **51**, 3728 (1969).
[45] S. Sastry, Nature (London) **409**, 300 (2001).
[46] F. Sciortino, W. Kob, and P. Tartaglia, Phys. Rev. Lett. **83**, 3214 (1999).
[47] M. P. Allen and D. J. Tildesley, *Computer Simulation of Liquids* (Oxford University Press, Oxford, 1987).
[48] W. G. Hoover, A. C. Hindmarsh, and B. L. Holian, J. Chem. Phys. **57**, 1980 (1972).
[49] M. Prasad and T. Sinno, Appl. Phys. Lett. **80**, 1951 (2002).
[50] M. Prasad and T. Sinno, Phys. Rev. B **68**, 045206 (2003).
[51] S. Takeda, Microsc. Res. Tech. **40**, 313 (1998).
[52] M. J. Aziz, Appl. Phys. Lett. **70**, 2810 (1997).
[53] S. J. Cook and P. Clancy, Phys. Rev. B **47**, 7686 (1993).
[54] J. Q. Broughton and X. P. Li, Phys. Rev. B **35**, 9120 (1987).
[55] LAMMPS, in http://lammps.sandia.gov/
[56] P. Calvo, A. Claverie, N. Cherkashin, B. Colombeau, Y. Lamrani, B. de Mauduita, and F. Cristiano, Nucl. Instrum. Methods Phys. Res. B **216**, 173 (2004).
[57] K. S. Jones, in *Properties of Crystalline Silicon*, edited by R. Hull (INSPEC, London, 1997), pp. 755–763.
[58] K. S. Jones, S. Prussin, and E. R. Weber, Appl. Phys. A **45**, 1 (1988).